Electrochemical and thermodynamic evaluation on corrosion inhibition of C38 steel in 1 M HCl by *Rumex* ethanolic extract

H.A. Al-Sharabi,[1,2] F. Bouhlal,[1] K. Bouiti,[1] N. Labjar,[1]* E. Al Zalaei,[3] A. Dahrouch,[3] G.A. Benabdellah,[1] M. El Mahi,[1] B. Benmessaoud,[4] E.M. Lotfi,[1] B. El Otmani[1] and S. El Hajjaji[3]

[1]Laboratory of Spectroscopy, Molecular Modeling, Materials, Nanomaterials, Water and Environment, CERNE2D, ENSAM, Mohammed V University in Rabat, Morocco
[2]Laboratory of chemistry, Jamal Abdulnasser High School, Ministry of Education, Yemen
[3]Laboratory of Spectroscopy, Molecular Modeling, Materials, Nanomaterials, Water and Environment, CERNE2D, Faculty of Sciences, Mohammed V University in Rabat, Morocco
[4]Environment, Materials and Sustainable Development Team – CERNE2D, EST, Mohammed V University in Rabat, Morocco
**E-mail: najoua.labjar@ensam.um5.ac.ma*

Abstract

Interdisciplinary research groups are interested in corrosion because it combines materials science, chemistry, physics, metallurgy, and chemical engineering. Corrosion is caused by the chemical and electrochemical action of an environment on metals and alloys. The consequences are severe in a variety of fields, particularly industry: production halts, replacement of corroded parts, accidents, and pollution risks are all common occurrences with potentially severe economic consequences. One of the most effective strategies for ensuring the protection of these metal materials in environments characterized by contact with aggressive acid media is the use of plant extracts as inhibitors. *Rumex* ethanolic extract is a novel green corrosion inhibitor for C38 steel in an acidic medium that is both inexpensive and environmentally friendly. *Rumex* extracted inhibitor (RNVLE) was used to overcome two major challenges for corrosion inhibitors: poor performance at high temperatures and low biodegradability. The extraction process by maceration produced a yield of 16%. Open circuit potential (OCP), electrochemical impedance spectroscopy (EIS), and polarization techniques were used to assess RNVLE's inhibition performance. It was shown that the inhibition efficiency increased with increasing inhibitor concentration and decreased slightly with temperature increase. The RNVLE adsorption process on the C38 steel surface was found to be spontaneous and obeyed to Langmuir isotherm at all studied temperatures. The associated adsorption thermodynamic parameters led to suggest the occurrence of physical adsorption of the RNVLE compounds on the C38 steel surface.

Received: January 19, 2022. Published: March 23, 2022 doi: 10.17675/2305-6894-2022-11-1-23

Keywords: *C38 steel, Rumex Nervosus Vahl leaves extract (RNVLE), EIS, Tafel, corrosion, 1 M HCl.*

1. Introduction

The problem of the corrosion phenomenon on an industrial scale is basically linked to the damage caused to metallic installations, which inevitably leads to economic losses regarding reparation, replacement and loss of products [1–3]. In terms of corrosion control of metals in aggressive environments, the use of inhibitors is a more effective, economical and practical method of implementation [4–6]. The effectiveness of inhibitors is often associated with physical or chemical adsorption [7, 8]. This is mainly related to the presence of heteroatoms (P, N, O and S), the multiple bonds, aromatic rings, the size of the molecules, the bond strength to the metal/alloy, the length of the carbon chain, and the nature of the metal surface, *etc.* [5, 9, 10].

Besides, the temperature effect is an important and considerable factor that affects the metallic behavior in acidic mediums, thereby affecting the interaction between the metallic surface and the inhibitor molecules. Regarding the interest of this factor in corrosion process, it is of great importance to understand and assess the corrosion behavior as a function of temperature [12–14].

Several studies have investigated the effect of temperature on the inhibition of steel corrosion in acidic mediums containing green inhibitors, for example Bouhlal *et al.* have revealed that the temperature declines the inhibition power of the hydro-alcoholic extract of used coffee grounds of C38 steel in 1 M HCl [2]. M.A. Deyab has studied the Seaweed extract as an inhibitor of mild carbon steel corrosion in saline water. The study showed that the seaweed extract inhibition power increases with concentration and deceases with the temperature rise [12, 13]. The study of Umoren *et al.* focused on the exploration of the aqueous extract from date palm leaves as a carbon steel corrosion inhibitor. The findings indicate that aqueous extract from date palm leaves has a great inhibition power. The inhibition efficiency has been found to rise with the concentration and decline with temperature [16]. Aqueous extract of Henna leaves has been studied as an inhibitor of carbon steel in 1 M HCl medium. The inhibition efficiency was found to increase with extract concentration and to decrease with temperature [12].

Rumex Nervosus Vahl (RNV) is a perennial herb in the *Rumex* genus, which is part of the *Polygonaceae* family. It grows in Yemen, Saudi Arabia, Ethiopia, Somalia, Kenya, and Tanzania, among other places. It's been used to treat a variety of inflammatory diseases in the past, including diarrhea, burns, typhus, rabies, and skin conditions [17]. It is known in Yemen as Al-Athrab (*Rumex Nervosus*) and is grown on a wide range of mountains and plains, particularly in the western and central regions, including Ibb, Taiz, Dhamar, Sana'a, and Al Mahwit [18].

The purpose of this study is to evaluate the inhibitory efficiency of ethanolic extract of *Rumex Nervosus Vahl* leaves on C38 steel corrosion in 1 M HCl solution at varying temperatures and different concentrations of our extract (RNVLE).

2. Experimental procedure

2.1. Plant extract preparation

The *Rumex* leaves (RNVL) were collected from IBB in central Yemen, dried at room temperature, and ground by hand. For 24 h, 50 g of powder was soaked in 100 mL of 99% ethanol solution. The final extract was filtered and evaporated in a rotary evaporator using filter paper. The extract was kept at 4°C in the refrigerator. The extraction yield was calculated using Equation 1 [8]:

$$Y = (m_{\text{ext}}/m_{\text{sample}}) \cdot 100 \quad (1)$$

where Y is the yield of extraction in %, m_{ext} is the mass of the extract after solvent evaporation in g, m_{sample} the dray mass of the specimen before extraction in g.

2.2. Electrode and solutions

The working electrode investigated in this study is a C38 steel with the following chemical composition (wt.%): C = 0.37; S = 0.016; Cr = 0.077; Mn = 0.68; Si = 0.23; Co = 0.009; Cu = 0.16; Ni = 0.059; Ti = 0.011 and the rest is iron (Fe). The working electrode was polished with a series of (SiC) emery papers (120, 400, 600, 1000, and 1200 grade), then soaked in distilled water and ultrasonically degreased in ethanol before each test. To make the 1 M HCl solution, a 37% HCl solution was diluted with bidistilled water (corrosive medium).

2.3. Electrochemical tests protocol

The electrochemical tests were performed using an VMP3 potentiostat associated with an EC-Lab software, the three-electrode cell was comprised of C38 steel specimen as working electrode (WE), a platinum wire as the counter electrode (CE) and a saturated calomel electrode (SCE) as a reference electrode (RE). Before each investigation, the open circuit potential (OCP) evolution was assessed for 30 min in order to reach a quasi-stationary value for the OCP. All assays were carried as function of extract concentration and at temperature ranging from 30 to 60°C. The voltage supplied to the specimens was continuously changed at a scan rate of (0.5 mV/sec) for Potentiodynamic polarization (PDP). All of the tests were carried out at ambient temperature. The inhibition effectiveness *IE*% is expressed by the (Equation 2), [14, 19]:

$$IE\% = \frac{i_{\text{corr}} - i_{\text{inh}}}{i_{\text{corr}}} \cdot 100 \quad (2)$$

where i_{corr} and i_{inh} are the C38 steel corrosion current density derived by extrapolating Tafel lines with and, without the inhibitor, respectively.

Electrochemical impedance spectroscopy plots were registered by swapping frequencies from 100 kHz to 10 mHz, the inhibitor's inhibition efficiency was calculated based on the charge transfer resistance values (Equation 3) [5, 10]:

$$IE\% = \frac{R_{\text{ctinh}} - R_{\text{ct}}}{R_{\text{ct}}} \cdot 100 \quad (3)$$

where R_{ctinh} and R_{ct} are respectively the values of the charge transfer resistances of the C38 steel in 1 M HCl with and without the different concentrations of RNVLE.

3. Results and Discussion

3.1. Extraction yield

One of the important factors that allow an overview of the economic feasibility is the yield percentage obtained from an extraction process. The extraction of *Rumex* leaves yielded a percentage of 16% in this study (Table 1), which is higher than other reported extract's yields.

Table 1. The yield obtained from extracting *Rumex* leaves and other plant extracts.

Vegetal material	Extraction method	Solvent	Yield (%)	Reference
Albizia lebbeck	Maceration	Ethanol	3.3	[20]
Aloe perryi	Maceration	Ethanol	12.6	[20]
Rumex leaves	Maceration	Ethanol	16	This work

3.2. Trace of open circuit potential

Based on the literature, the OCP stability, before each polarization or impedance measurement, acquired special importance [21]. Furthermore, the OCP evolution as function of time provides important information about the corrosion domains, complete or partial inhibition, and about inhibitor concentrations [6, 22].

At all the studied temperatures, the OCP progresses towards steady values, this is true for all the investigated extract concentrations [23]. A steady state of OCP evolution has been quickly reached before 30 min. Similar behavior has been previously reported in the literature. As can be observed from Figure 1, there is no correlation between the OCP evolution and the extract concentration. This kind of comportment may be due to a mixed-type inhibition of corrosion. We can also see in the graph that there is a correlation slight between temperature rise and the development of E_{OCP} [24].

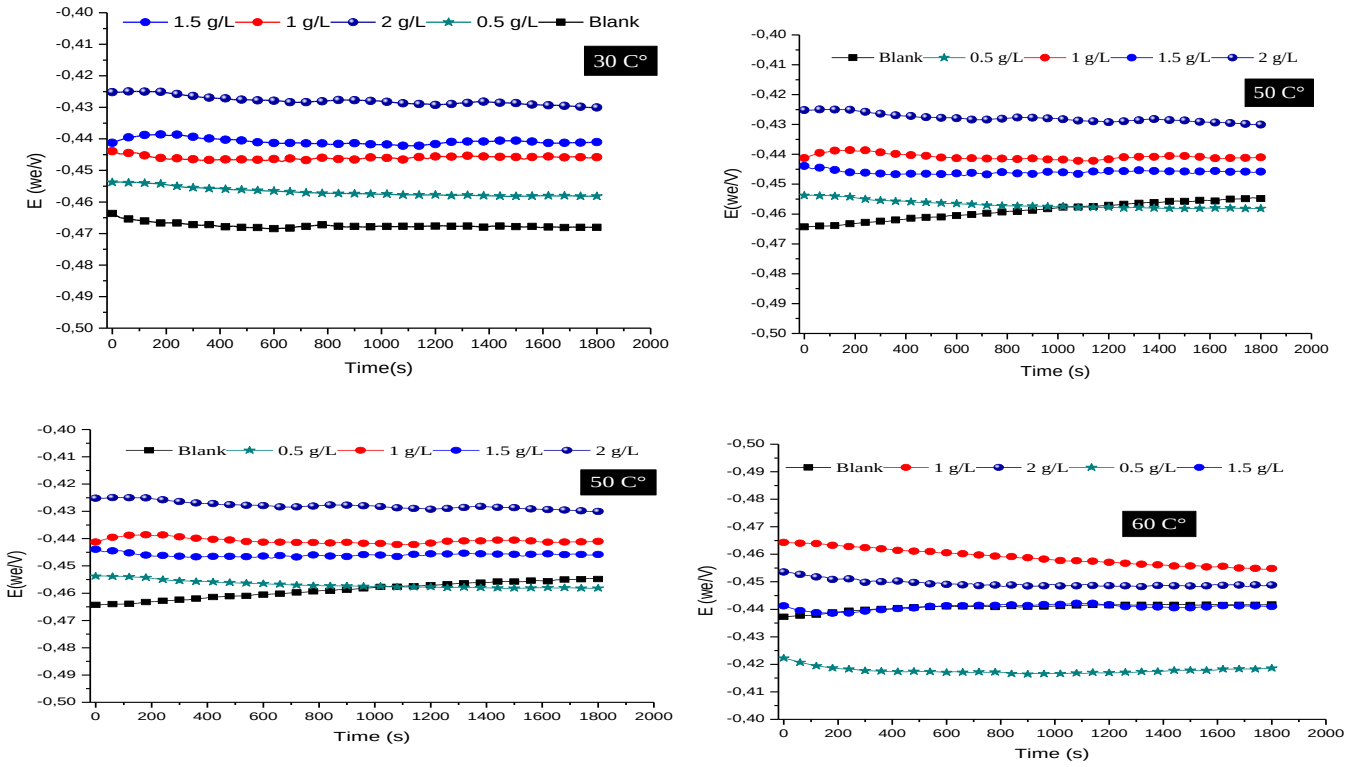

Figure 1. E_{OCP} as a function of immersion time, and temperature 30–60°C.

3.3. Potentiodynamic polarization investigation (PDP)

The polarization curves method was used to evaluate the temperature effect on the RNVLE's inhibition action on C38 steel corrosion [21]. The tests were carried out at various temperatures (30–60°C) in 1 M HCl without and with varying concentrations of RNVLE. As according to Figure 2, the presence of the RNVLE inhibitor inhibits both anodic and cathodic reactions. This lends credence to the fact that the RNVLE prevents C38 steel corrosion by controlling both anodic and cathodic reactions (mixed type inhibitor) [23]. Examining Figure 2, we can see that the inhibitory effect was more visible in the cathodic part, whereas it appears in the anodic part that after –0.3 mV, the inhibitory effect begins to fade, as there is a clear increase in the curves of increasing concentrations, and this is due to the fact that the adsorption process is parallel to the absorption process. This process becomes clearer with increasing temperature which is evident in that change [8]. Table 2 clearly shows the electrochemical kinetic parameters corrosion potential (E_{corr}), corrosion current density (I_{corr}), and cathodic Tafel slopes (β_c, β_a) determined by extrapolation from these experiments. I_{corr} values are used to calculate inhibition efficiencies, *IE*%. The surface coverage was [13] calculated by using the Equation below:

$$\theta = (i^0_{corr} - i^{inh}_{corr})/i^0_{corr} \quad (4)$$

where i^0_{corr} and i^{inh}_{corr} are the corrosion uninhibited and inhibited current density, respectively.

An increase in temperature will increase hydrogen production at the cathode, which increases the conversion of iron atoms at the anode and their transformation into ions dissolved in the solution [25], resulting in an increase in the current passing through the electrolysis cell, which is reflected on the inhibition efficiency according to Equation 1, as shown in Figure 2 and Table 2.

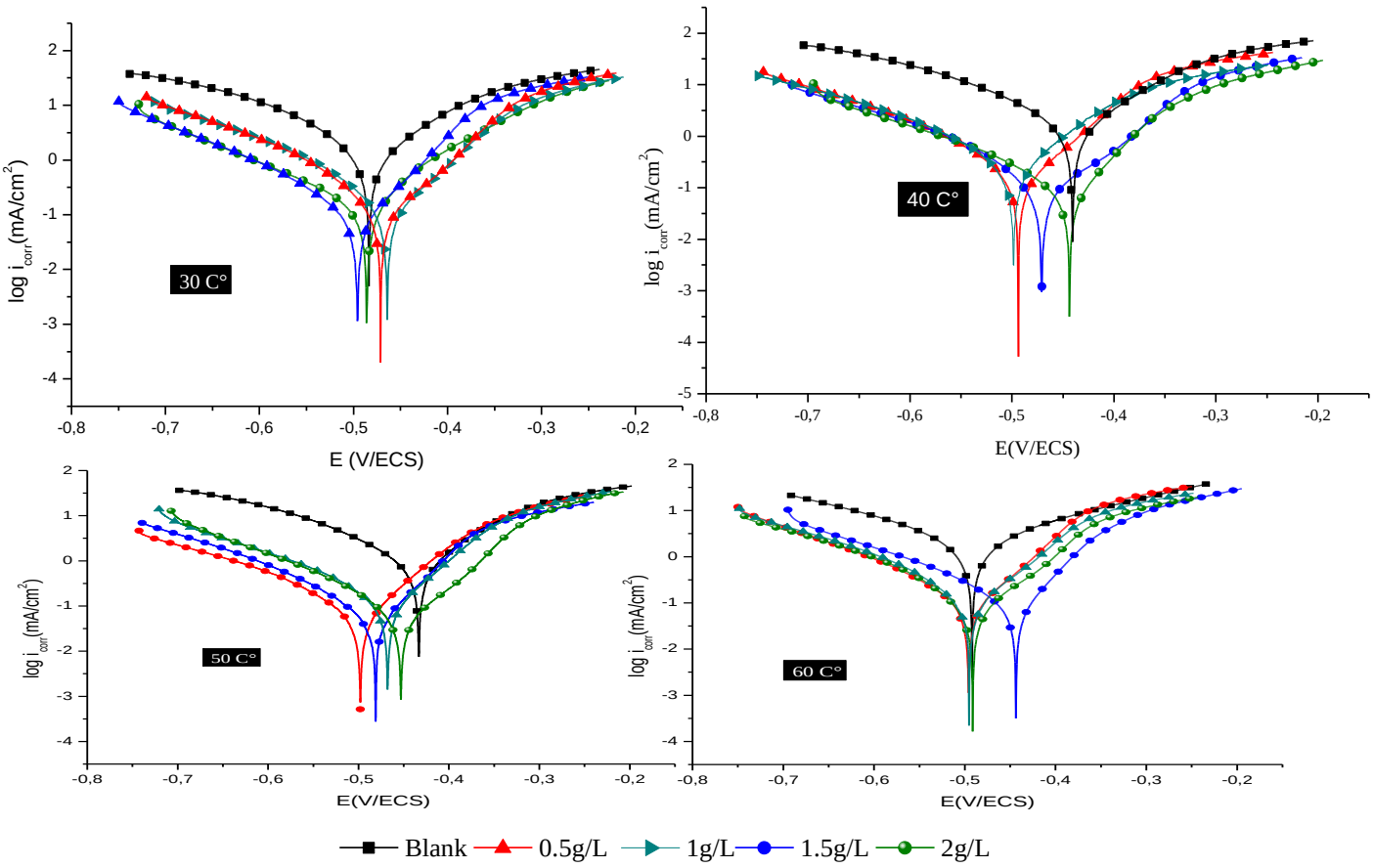

Figure 2. Tafel plots for C38 in 1 M HCl without and with 0.5–2 g/L RNVLE at 30–60°C.

Table 2. Tafel Parameters and inhibitory efficiency of C38 corrosion in 1 M HCl solution with different concentrations of the RNVLE at various temperatures (30 to 60°C).

Temperature (°C)	Concentration (g/L)	$-E_{corr}$ (mV/SCE)	I_{corr} (μA/cm^2)	β_a (mV)	$-\beta_c$ (mV)	IEPDP (%)	θ
30	Blank	433.3	974.6	99.4	130.6	–	–
	0.5	467.8	122.1	71.9	119.5	87.5	0.875
	1	467.8	102.3	66.0	101.0	89.5	0.895
	1.5	497.9	80.4	69.7	111.8	91.7	0.917
	2	453.5	45.5	58.9	101.7	95.3	0.953

Temperature (°C)	Concentration (g/L)	$-E_{corr}$ (mV/SCE)	I_{corr} (μA/cm^2)	β_a (mV)	$-\beta_c$ (mV)	IEPDP (%)	θ
40	Blank	464.8	1025.4	111.5	121.5	–	–
	0.5	495.7	152.9	94.9	139.1	85.1	0.851
	1	495.3	124.2	79.9	119.7	87.9	0.879
	1.5	496.5	100.1	68.2	116.8	90.2	0.902
	2	470.8	68.8	69.8	79.5	93.3	0.933
50	Blank	483.6	1645.4	126.9	135.8	–	–
	0.5	486.0	280.9	105.8	172.4	82.9	0.829
	1	464.3	205.3	95.8	120.0	87.5	0.875
	1.5	495.7	165.3	66.7	106.7	89.9	0.899
	2	471.1	148.6	85.3	112.3	90.9	0.909
60	Blank	440.5	2029.8	113.1	143.0	–	–
	0.5	498.7	454.9	111.7	154.9	77.6	0.776
	1	474.5	353.7	92.1	135.5	82.6	0.826
	1.5	485.9	280.3	83.2	110.4	86.2	0.862
	2	470.8	205.2	82.8	122.5	89.9	0.899

Table 2 shows that, for both uninhibited and inhibited solutions, the inhibition efficiency of RNVLE increases with increasing concentration and decreases slightly with increasing temperature within the studied experimental limits. The aggressiveness of the corrosive medium is expected to increase as the temperature rises [1, 13]. Accordingly, the inhibition efficiency decreases. This could be a sign of RNVLE's physical adsorption mechanism on a metal surface. On the other hand, RNVLE may continue to adsorb strongly and act as a corrosion inhibitor for C38 steel. At a temperature of 60°C, *IE*% was maintained at 90.9% with 2 g/L RNVLE. The increase in current passing through the corrosion cell is clearly influenced by the increase in temperature in the blank solution, and adding *Rumex* extract concentrations causes it to decrease, confirming *Rumex* extract's effectiveness. Figure 3 depicts the changes that occurred as concentration and temperature increased.

3.4. Electrochemical Impedance Spectroscopy (EIS) study

EIS was used to investigate the corrosion behavior of C38 steel in 1 M HCl solution in the presence of various concentrations of RVNL extract in the temperature range of 30–60°C. Figures 3 and 4 show the impedance plots (Nyquist and Bode) of a C38 steel electrode in a 1 M HCl solution with different concentrations of RNVLE at 30–60°C [26, 27]. The shape of the Nyquist plots indicate that charge transfer primarily controls the corrosion process. The presence of RNVLE increased the size of the impedance plots, implying that the organic

compounds in the RNVLE formed a protective film on the C38 surface. The capacitive loop increased with increasing inhibitor concentration as more inhibitor molecules adsorbed on the steel surface, indicating that the inhibitor film gradually compacted and, as a result, provided better protection [21, 28, 29]. Furthermore, as the temperature increases, the size of the capacitive loop decrease, implying that high temperatures accelerated corrosion. Despite this, the addition of RNVLE significantly increased the size of the spectra in comparison to the blank solution, demonstrating RNVLE's high inhibitive ability at temperatures under study 30–60°C [12]. These findings revealed the formation of an inhibitor-adsorption film on the steel surface, as well as its contribution to the improved anti-corrosive quality [30].

The overall shape of the Bode diagrams (Figure 4) is similar in both cases (absence and presence of the inhibitor), it is the same for all concentrations and temperatures studied. This indicates that the addition of the inhibitor has no effect on the corrosion mechanism [31].

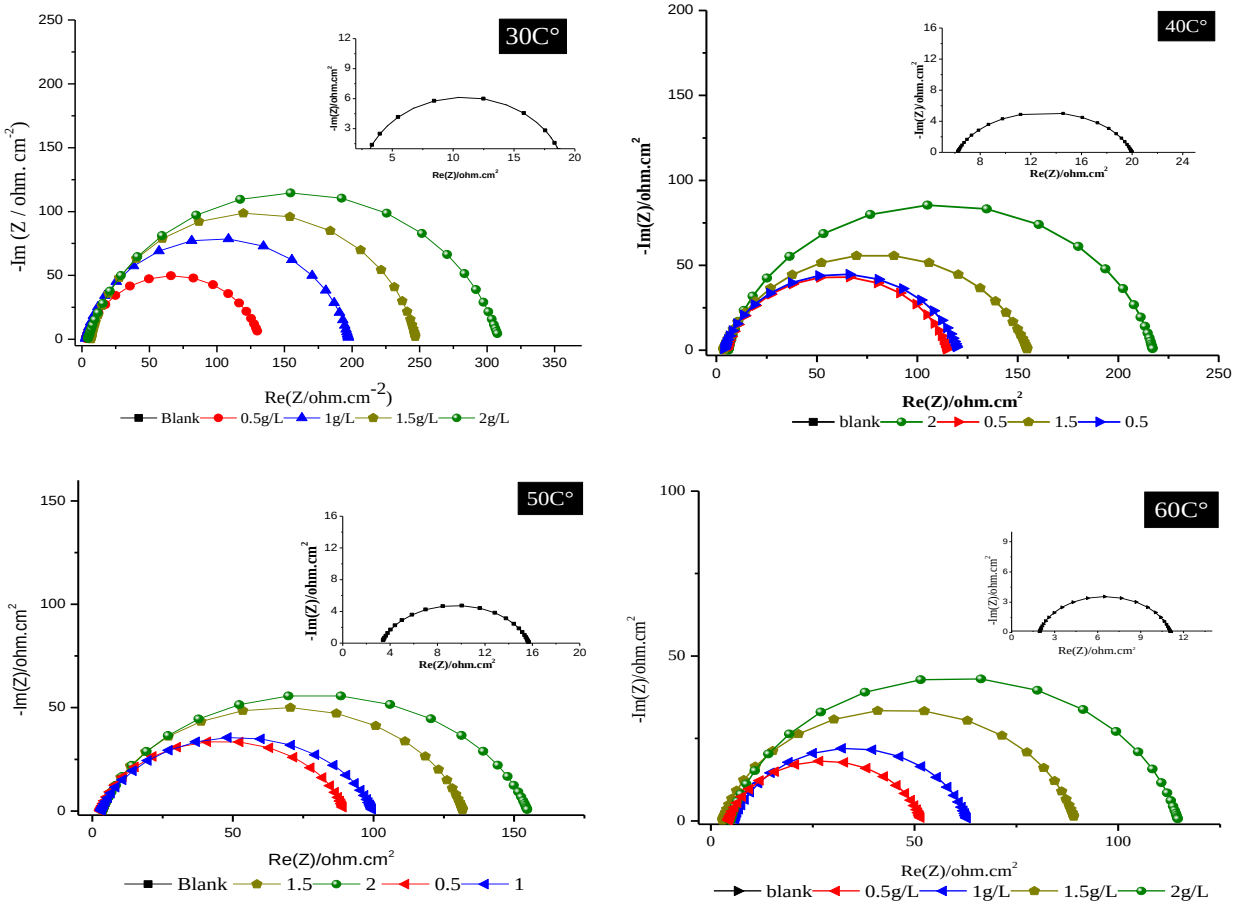

Figure 3. Nyquist plots for C38 in 1 M HCl (blank) and with (0.5–2 g/L) of RNVLE at 30–60°C.

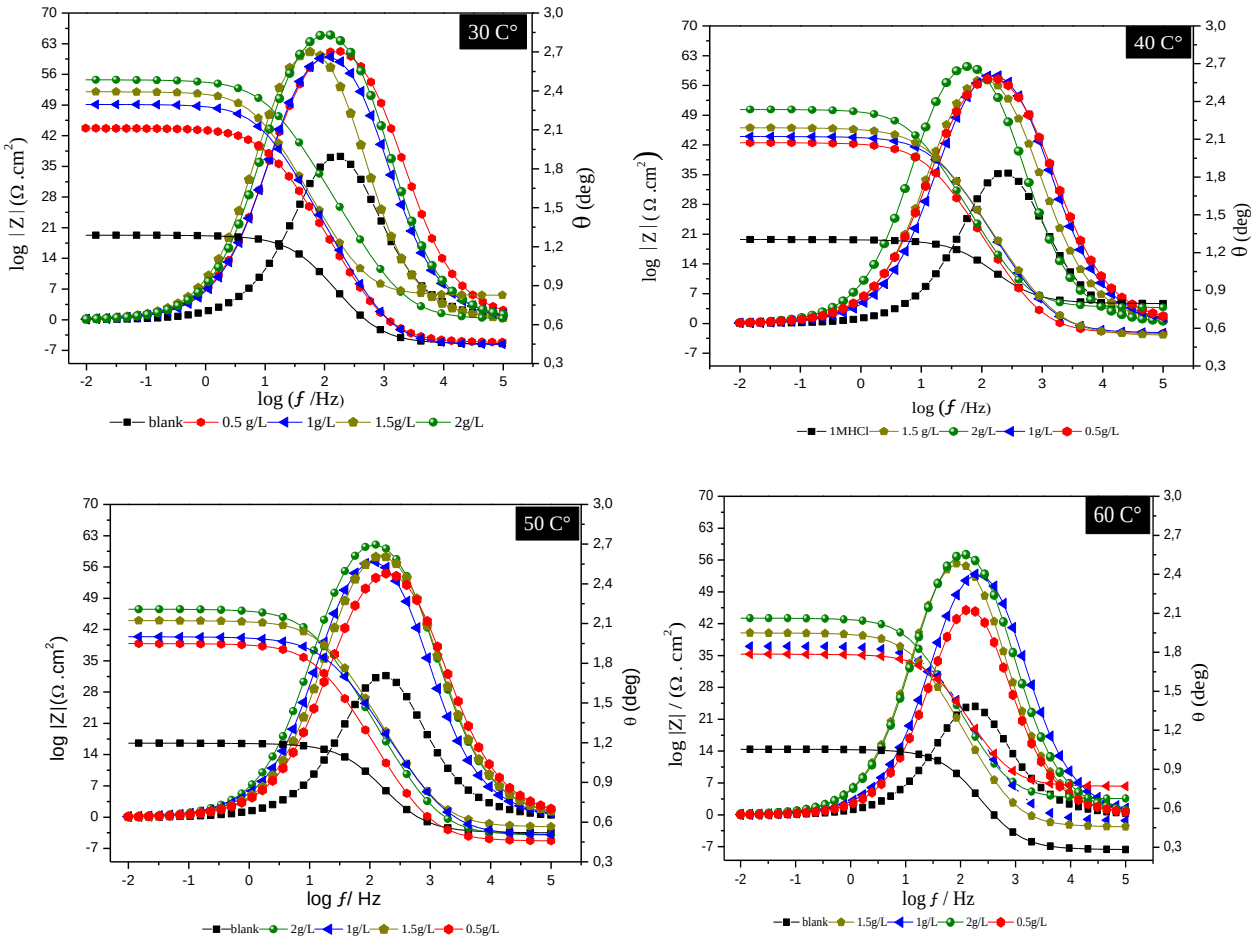

Figure 4. Bod plots for C38 in 1 M HCl blank and with (0.5–2g/L) of RNVLE at 30–60°C.

All of the spectra were well modeled by adjusting the experimental points by an equivalent circuit shown in Figure 5. Tables 3 and 4 compile the electrical parameters determined by adjusting the experimental data. Table 3 displays the electrochemical parameters along with the inhibitory efficiency, demonstrating clearly that our inhibitor works well at the temperatures studied, with a slight decrease as the temperature is increased. Also, Table 3 displays the value a_2 which indicates the surface inhomogeneity resulting from surface metal roughening and/or formation of corrosion products on the surface, X^2 is a coefficient of validating this model.

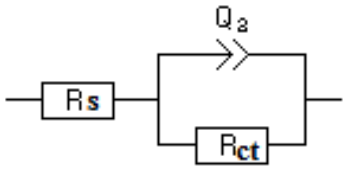

Figure 5. Equivalent circuits used to fit the EIS data.

The solution resistance is R_s, R_{ct} is the charge-transfer resistance, and Q_2 is the constant phase element that represents the capacitance of the double layer at the metal/solution interface in this circuit. Between "*Q*" and "pure capacitance", there is usually a phase shift [21]. As a result, by replacing the capacitor *C* with a constant phase element, impedance spectra can be simulated (CPE). The CPE's impedance is described by the equation below [32]:

$$Z_{CPE} = Q^{-1}(j\omega)^n \quad (5)$$

where *Q* (in Ω^{-1} S^n cm^{-2}), $j^2 = -1$ (in rad s^{-1}), ω and *n* are the CPE constant, imaginary number, angular frequency, and CPE exponent that can be used to determine the surface heterogeneity or roughness.

Table 3. EIS parameters and inhibitory efficiency of C38 steel corrosion in a 1 M HCl solution blank and with various concentrations of the *Rumex* extract.

T **(°C)**	**Concentration (g/L)**	R_S **(Ohm·cm²)**	Q_2 **(e⁻³ F·cm⁻²)**	a_2	R_{ct} **(Ohm·cm²)**	X^2	***IE*%**
	Blank	2.8±0.4	$0.5\pm(0.3\cdot10^{-3})$	0.83±0.6	16.32±0.5	$6.8\cdot10^{-3}$	–
	0.5	2.8±0.8	$0.2\pm(14.1\cdot10^{-3})$	0.83±0.5	129.2±0.6	$6.1\cdot10^{-3}$	87.4
30	1	2.7±0.3	$0.2\pm(4.7\cdot10^{-3})$	0.86±0.5	194.9±0.6	$1.2\cdot10^{-2}$	91.6
	1.5	3.7±0.3	$0.1\pm(2.2\cdot10^{-3})$	0.87±0.5	240.6±0.5	$2.3\cdot10^{-2}$	93.2
	2	3.4±0.3	$0.1\pm(2.8\cdot10^{-3})$	0.85±0.5	304.5±0.5	$3.0\cdot10^{-2}$	94.6
	Blank	3.2±0.4	$0.4\pm(0.3\cdot10^{-3})$	0.81±0.7	13.8±0.5	$8.6\cdot10^{-3}$	–
	0.5	4.7±0.3	$0.2\pm(12.1\cdot10^{-3})$	0.83±0.5	108.0±0.6	$1.0\cdot10^{-2}$	87.2
40	1	3.9±0.4	$0.2\pm(0.5\cdot10^{-3})$	0.83±0.5	116.4±0.6	$3.7\cdot10^{-2}$	88.1
	1.5	3.5±0.3	$0.2\pm(7.2\cdot10^{-3})$	0.81±0.5	151.4±0.5	$1.3\cdot10^{-2}$	90.9
	2	3.8±0.3	$0.2\pm(4.7\cdot10^{-3})$	0.86±0.5	211.5±0.5	$3.6\cdot10^{-2}$	93.5
50	Blank	3.3±0.3	$0.5\pm(0.3\cdot10^{-3})$	0.82±0.6	12.4±0.5	$8.2\cdot10^{-3}$	–
	0.5	4.7±0.3	$0.2\pm(12.7\cdot10^{-3})$	0.85±0.5	86.8±0.5	$1.5\cdot10^{-2}$	85.7
	1	3.2±0.3	$0.2\pm(14.1\cdot10^{-3})$	0.81±0.5	96.7±0.6	$1.9\cdot10^{-2}$	87.2
	1.5	3.4±0.4	$0.1\pm(4.7\cdot10^{-3})$	0.87±0.5	130.4±0.6	$1.2\cdot10^{-2}$	90.4
	2	4.3±0.4	$0.2\pm(6.8\cdot10^{-3})$	0.86±0.5	156.5±0.6	$4.1\cdot10^{-2}$	92.1
60	Blank	3.6±0.5	$0.6\pm(0.3\cdot10^{-3})$	0.83±0.5	9.2±0.5	$7.6\cdot10^{-2}$	–
	0.5	4.3±0.4	$0.2\pm(45.9\cdot10^{-3})$	0.83±0.6	47.5±0.5	$4.8\cdot10^{-3}$	80.6
	1	3.2±0.3	$0.2\pm(20.1\cdot10^{-3})$	0.83±0.5	67.7±0.5	$7.5\cdot10^{-3}$	86.3
	1.5	3.8±0.3	$0.2\pm(22.1\cdot10^{-3})$	0.82±0.5	86.6±0.6	$2.1\cdot10^{-2}$	89.4
	2	4.7±0.3	$0.2\pm(12.8\cdot10^{-3})$	0.85±0.5	110.0±0.6	$4.1\cdot10^{-2}$	91.6

Table 4. Bode parameters for C38 in 1 M HCl containing (0.5–2 g/L) of RNVLE at 30–60°C.

***T* (°C)**	**Concentration (g/L)**	**θ_{max} (deg)**	***Freq*$_{(max)}$ (Hz)**	**Slope**
30	Blank	37.2	2.3	0.39
	0.5	59.9	2.1	0.68
	1	60.1	1.8	0.74
	1.5	61.2	2.3	0.67
	2	64.9	2.1	0.69
40	Blank	35.3	2.3	0.24
	0.5	57.3	2.1	0.59
	1	57.7	2.1	0.62
	1.5	58.3	2.3	0.62
	2	60.4	1.9	0.56
50	Blank	31.6	2.3	0.31
	0.5	54.5	2.1	0.63
	1	57.1	2.1	0.59
	1.5	58.3	2.3	0.65
	2	60.2	2.2	0.68
60	Blank	23.5	2.4	0.33
	0.5	44.9	2.1	0.46
	1	52.8	1.9	0.54
	1.5	55.2	2.1	0.62
	2	57.2	2.2	0.59

From Figure 4 one time constant was observed for all concentrations and temperatures. Additionally, it can be clearly seen that the maximum phase the angle increases with the rise of RNVLE concentration, which may be due to the inhibitor's adsorption on the steel surface. A linear relationship between log|*Z*| *versus* log(*Freq*) has also been noted. Table 4 shows the values of the slopes of the Bode plots at intermediate frequencies, the maximum phase angles (θ_{max}) and the corresponding frequencies ($Freq_{max}$) for C38 steel in 1 M HCl solution containing different concentrations of RNVLE at different temperatures [28, 33].

3.5 Adsorption isotherm and thermodynamic calculation

Adsorption isotherms can be used to describe the mechanism of adsorption and interaction between RNVLE and the C38 surface. When the corrosion rate is reduced in the presence of the inhibitor, quasi-equilibrium adsorption occurs, which can be studied using adsorption

isotherms [34]. Langmuir is the isotherm that has the best agreement with our experimental data and can be expressed using Equation 6 [35]:

$$\frac{C_{\text{inh}}}{\theta} = \frac{1}{K_{\text{ads}}} + C_{\text{inh}} \tag{6}$$

where C, θ and K_{ads} are the RNVLE concentration, surface coverage, and adsorption equilibrium constant, which can be determined by plotting C/θ *versus* C at different temperatures (Figure 6). Equation 7 can be used to calculate the standard Gibbs free energy change of adsorption (ΔG^0_{ads})[22, 36].

$$\Delta G^0_{\text{ads}} = -2.303RT\log(55.5K_{\text{ads}}) \tag{7}$$

where T is the temperature, R is 8.314 J·mol^{-1}·K^{-1}, and 55.5 is the number of moles of water in one liter. Table 4 shows the K_{ads} and ΔG^0_{ads} values for RNVLE adsorption on the C38 surface.

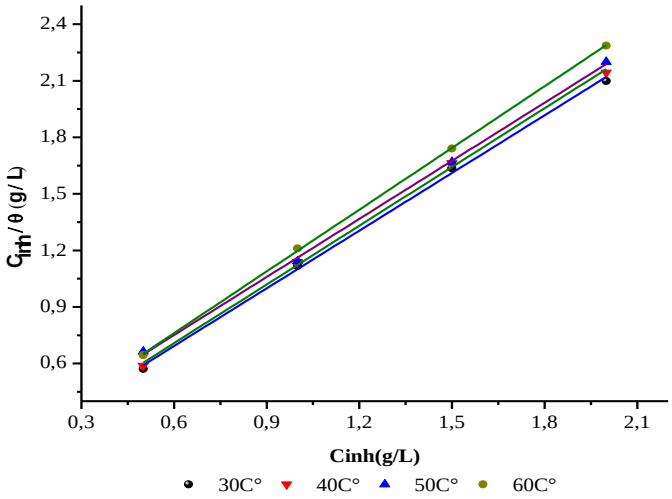

Figure 6. Langmuir isotherms for C38 in 1 M HCl in the presence of RNVLE at 30–60°C.

Table 4. Thermodynamic parameters for the adsorption of RNVLE on C38 surface in 1 M HCl.

Temperature (°C)	**Slope**	K_{ads} **(mol^{-1})**	ΔG^0_{ads} **(KJ/mol)**	R^2
30	1.02002	12.4	–16.2	0.998
40	1.03872	11.8	–16.1	0.998
50	1.0917	9.4	–15.5	0.999
60	1.02728	7.4	–14.9	0.999

As shown in Table 4, the K_{ads} values decrease with temperature, implying that corrosion is intensifying and thus limiting the RNVLE's ability to adsorb on the C38 steel surface.

Negative values of the standard free adsorption energy, as shown in Table 4 indicate spontaneous adsorption of extract compounds on the C38 steel surface. The absolute values of ΔG^0_{ads} listed are less than 20 KJ mol^{-1}, indicating that RNVLE adsorption on the C38 surface occurred primarily through a physical adsorption mechanism [8]. This type of adsorption involves an electrostatic interaction between a charged molecule and a charged metal, which is highly sensitive to thermal agitation and breaks easily as the latter rises [11].

Thermodynamically, (ΔG^0_{ads}) is linked to the standard enthalpy and entropy of the adsorption process, ΔH^0_{ads} and ΔS^0_{ads} respectively, *via* Equation 8:

$$\Delta G^0_{ads} = \Delta H^0_{ads} - T\Delta S^0_{ads} \quad (8)$$

The evolution of ΔG^0_{ads} as a function of temperature (°C) is linear, denoting that the thermodynamic parameters are well correlated (Figure 7). Table displays the thermodynamic data obtained for RNVLE.

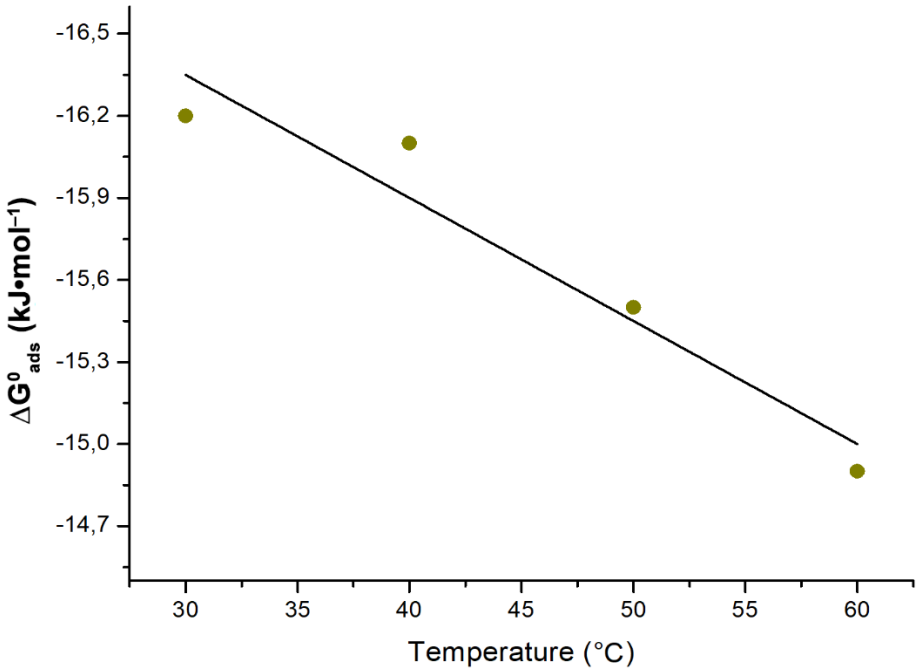

Figure 7. The evolution of ΔG^0_{ads} as a function of temperature.

Table 5. ΔH^0_{ads} and ΔS^0_{ads} values obtained from the linear relationship between free energy and temperature.

Temperature (°C)	ΔG^0_{ads} **(kJ·mol^{-1})**	ΔH^0_{ads} **(kJ·mol^{-1})**	ΔS^0_{ads} **(J·mol^{-1}·K^{-1})**
30	–16.2	–45.0	–177.2
40	–16.1		
50	–15.5		
60	–14.9		

Furthermore, the value (ΔH^0_{ads}) provides important information about the inhibitor's adsorption mechanism. Endothermic adsorption ($\Delta H^0_{ads}>0$) is explicitly attributed to chemisorption [34], whereas exothermic adsorption ($\Delta H^0_{ads}<0$) may involve physisorption and/or chemisorption. In the literature, absolute values of ΔH^0_{ads} less than 40 kJ·mol^{-1} indicate physisorption, while absolute values of ΔH^0_{ads} greater than (100 kJ·mol^{-1}) indicate chemisorption [37, 38]. In our case, the absolute value of ΔH^0_{ads} discovered is in the order of (–45.0 kJ·mol^{-1}), which is both close to the absolute value of ΔH^0_{ads} involving physisorption and much lower than the absolute value of ΔH^0_{ads} involving chemisorption, indicating that this inhibitor is physisorbed on the steel surface. Table 5 also shows the value of (ΔS^0_{ads}), which is negative (–177.2), confirming that the RNVLE adsorption process follows the physical type [28, 29].

3.6. Corrosion activation parameters

The activation energy (E_a) has a direct impact on the corrosion inhibition mechanism and the efficiency of RNVLE. Temperature is a critical factor in the corrosion process because it increases the rate of chemical reactions [36]. Furthermore, RNVL's adsorption can change the activation energy of anodic or cathodic reactions in inhibited systems. As a result, the apparent activation energy was calculated using the [36] Arrhenius Equation 9.

$$\ln i_{corr} = \ln A - \frac{E_a}{RT} \tag{9}$$

where i_{corr}, A, R, and T are corrosion current density, the Arrhenius constant, the gas constant, and the experimental temperature, respectively.

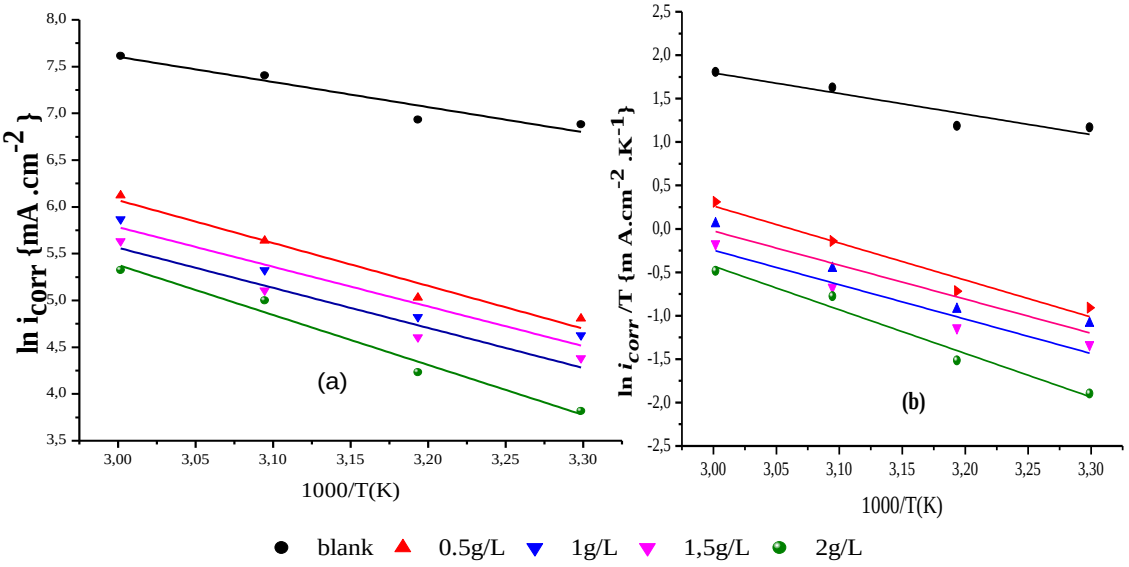

Figure 8. Activation plots (a) and transition-state plots (b) of C38 without and with 0.5–2 g/L of RNVLE.

The slope of $\ln i_{corr}$ *versus* $1/T$ plots (Figure 8) with and without RNVLE can be used to calculate E_a, and its values are listed in Table 5. At all concentrations, the E_a values for the RNVLE systems are higher than the blank system, indicating physical adsorption of the inhibitor on the steel surface. This means that in the presence of the RNVLE, the corrosion reaction's energy barrier rises.

Table 5. Activation energy parameters of C38 in 1 M HCl and with 0.5–2 g/L of RNVLE.

Concentration (g/L)	E_a **(kJ·mol^{-1})**	ΔH_a^0 **(kJ·mol^{-1})**	ΔS_a^0 **(J·mol^{-1})**	$E_a - \Delta H_a^0$ **(J·mol^{-1}·K^{-1})**
Blank	22.35	19.72	–170.8	2.63
0.5	35.25	32.61	–147.9	2.64
1	35.61	32.97	–147.2	2.64
1.5	38.08	35.44	–136.3	2.64
2	44.40	41.78	–123.1	2.62

The following equation can be used to calculate other thermodynamic parameters such as enthalpy and entropy [12, 15]:

$$i_{corr} = RT/Nh \cdot \exp(\Delta S_{ads}^0/R) \cdot \exp(\Delta H_{ads}^0/RT) \quad (10)$$

where N denotes Avogadro's number and h denotes Planck's constant. ΔH_{ads}^0 and ΔS_{ads}^0 are calculated using the slope and intercept of the plots shown in (Figure 9b), and the results are presented in Table 5.

The positive value of enthalpy of activation in the absence and presence of various inhibitor concentrations reflects the endothermic nature of the C38 steel dissolution process, indicating that steel dissolution is difficult [35]. However, all activation energies (E_a) values are greater than analogous ΔH_{ads}^0 values, indicating that the corrosion process involves a gaseous reaction, that of H_2 formation [36]. Furthermore, for all systems, the mean value of the difference ($E_a - \Delta H_a^0$) is approximately 2.64 kJ/mol (Figure 10), which is close to the mean value of the product RT (2.68 kJ/mol) when T is between 30 and 60°C this is explained by the fact that the corrosion process is a unimolecular reaction, as described by the following Equation:

$$E_a - \Delta H_a^0 = RT \quad (11)$$

Table 5 shows that the value increased in the presence of the inhibitor compared to the uninhibited solution, indicating a higher level of protection it can be explained as follows in the free acid solution: the rate-determining recombination step's transition state represents a more orderly arrangement than the initial state, resulting in a high negative value for activation entropy ΔS_a^0. The rate-determining step in the presence of an inhibitor, however, is the discharge of hydrogen ions to form adsorbed hydrogen atoms. Because the metal

surface is covered with inhibitor molecules, the discharge of hydrogen ions at the metal surface is slowed, causing the system to move away from a random arrangement, increasing the entropy of activation. As a result, the entropy of activation increases (in the presence of inhibitors, the disordering from reactant to activated complex increases) [13, 15].

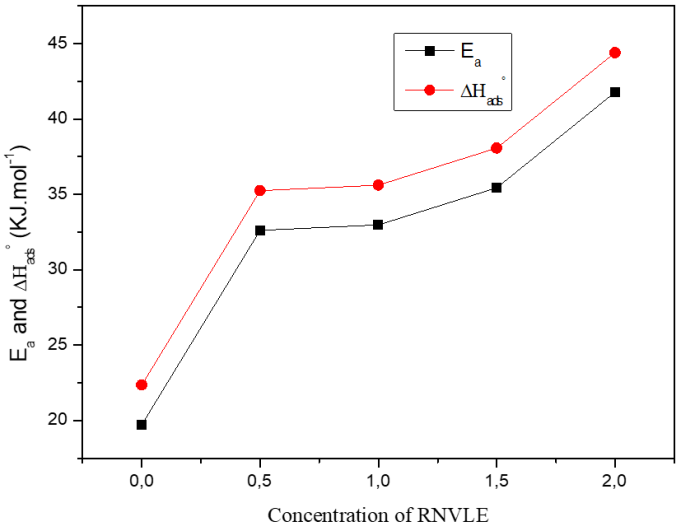

Figure 9. Relationship between E_a and a ΔG^0_{ads} and RNVLE concentration.

Conclusion

The inhibition efficiency increased with increasing RNVLE concentration and decreased slightly with increasing temperature. At a concentration of 2 g/L, a high inhibition efficiency has been obtained for (IE_Z = 94.6%) at 30°C, at the same concentration, we obtained a 91% inhibition efficiency at 60°C. Furthermore, the Potentiodynamic polarization and impedance measurements show that RNVLE is a mixed-type inhibitor, affecting both the anodic and cathodic processes by simply blocking the metal's active sites and a charge-transfer process governs the corrosion process. The Langmuir adsorption isotherm more accurately describes the experimental results reported in this paper. The negative ΔG^0_a values indicate that the inhibitors adsorb spontaneously on the surface of the C38 steel.

The thermodynamic values obtained from this study, and E_a, ΔH^0, and ΔS^0 indicate that the presence of the inhibitor increases the activation energy.

References

1. T. Douadi, H. Hamani, D. Daoud, M. Al-noaimi and S. Chafaa, Effect of temperature and hydrodynamic conditions on corrosion inhibition of an azomethine compounds for mild steel in 1 M HCl solution, *J. Taiwan Inst. Chem. Eng*., 2016, **71**, 388–404. doi: 10.1016/j.jtice.2016.11.026

2. F. Bouhlal, N. Labjar, F. Abdoun, A. Mazkour, M. Serghini-Idrissi, M. El Mahi and S. El Hajjaji, Electrochemical and Thermodynamic Investigation on Corrosion Inhibition of C38 Steel in 1M Hydrochloric Acid Using the Hydro-Alcoholic Extract of Used Coffee Grounds, *Int. J. Corros*., 2020, **2020**, 4045802. doi: 10.1155/2020/4045802
3. W. Belmaghraoui, A. Mazkour, H. Harhar, M. Harir, and S. El Hajjaji, Investigation of corrosion inhibition of C38 steel in 5.5 M H3PO4 solution using Ziziphus lotus oil extract: an application model, *Anti-Corros. Methods Mater*., 2019, **66**, 121–126. doi: 10.1108/ACMM-02-2018-1901
4. R. Javaherdashti, How corrosion affects industry and life, *Anti-Corros. Methods Mater*., 2000, **47**, 30–34, doi: 10.1108/00035590010310003
5. O. Benali, M. Zebida and U. Maschke, Synthesis and inhibition corrosion effect of two thiazole derivatives for carbon steel in 1 M HCl, *J. Indian Chem. Soc*., 2021, **98**, 100113. doi: 10.1016/j.jics.2021.100113
6. M.A. Amain, P.I. Weight, S.S.A. El-Rehim and R.S. Bayoumi, The inhibition of low carbon steel corrosion in hydrochloric acid solutions by succinic acid, *Electrochim. Acta*, 2007, **52**, 3588–3600. doi: 10.1016/j.electacta.2006.10.019
7. R. Karthikaiselvi and S. Subhashini, Study of adsorption properties and inhibition of mild steel corrosion in hydrochloric acid media by water soluble composite poly (vinyl alcohol-o-methoxy aniline, *J. Assoc. Arab Univ. Basic Appl. Sci*., 2014, **16**, 74–82. doi: 10.1016/j.jaubas.2013.06.002
8. F. Bouhlal, N. Labjar, F. Abdoun, A. Mazkour, M. Serghini-Idrissi, M. El Mahi and S. El Hajjaji, Chemical and electrochemical studies of the inhibition performance of hydro-alcoholic extract of used coffee grounds (HECG) for the corrosion of C38 steel in 1M hydrochloric acid, *Egypt. J. Pet*., 2020, **29**, 45–52. doi: 10.1016/j.ejpe.2019.10.003
9. A. Soni, *Studies of hydroxytriazenes as corrosion inhibitors for brass*, Mohan Lal Sukhadia University, Department of Chemistry, Created and maintained by INFLIBNET Centre, 2016, 260. http://hdl.handle.net/10603/147848
10. Y. El Hamdouni, F. Bouhlal, H. Kouri, M. Chellouli, M. Benmessaoud, A. Dahrouch, and S. El Hajjaji, Use of Omeprazole as Inhibitor for C38 Steel Corrosion in 1.0M H_3PO_4 Medium, *J. Fail. Anal. Prev*., 2020, **20**, 563–571. doi: 10.1007/s11668-020-00862-5
11. F. Atabaki, S. Jahangiri and Z. Pahnavar, Thermodynamic and Electrochemical Investigations of Poly (Methyl Methacrylate–Maleic Anhydride) as Corrosion Inhibitors for Mild Steel in 0.5 M HCl, *Prot. Met. Phys. Chem. Surf*., 2019, **55**, 1161–1172. doi: 10.1134/S2070205119060030
12. A. Hamdy and N.S. El-Gendy, Thermodynamic, adsorption and electrochemical studies for corrosion inhibition of carbon steel by henna extract in acid medium, *Egypt. J. Pet*., 2013, **22**, 17–25. doi: 10.1016/j.ejpe.2012.06.002
13. N. Labjar, F. Bentiss, M. Lebrini and C. Jama, Study of temperature effect on the corrosion inhibition of C38 carbon steel using amino-tris (methylenephosphonic) acid in hydrochloric acid solution, *Int. J. Corros*., 2011, **2011**, 548528. doi: 10.1155/2011/548528

14. M.A. Deyab, Inhibition activity of Seaweed extract for mild carbon steel corrosion in saline formation water, *Desalination*, 2016, **384**, 60–67. doi: 10.1016/j.desal.2016.02.001
15. O. Sanni, A.P.I. Popoola and O.S.I. Fayomi, Temperature Effect, Activation Energies and Adsorption Studies of Waste Material as Stainless Steel Corrosion Inhibitor in Sulphuric Acid 0.5 M, *J. Bio Tribo Corros*., 2019, **5**, 88. doi: 10.1007/s40735-019-0280-2
16. S.A. Umoren, Z.M. Gasem and I.B. Obot, Date palm (Phoenix dactylifera) leaf extract as an eco-friendly corrosion inhibitor for carbon steel in 1M hydrochloric acid solution, *Anti-Corros. Meth. Mater*., 2015, **62**, 19–28. doi: 10.1108/ACMM-10-2013-1302
17. N.A. Al Yahya, S.A. Alrumman and M.F. Moustafa, Phytochemicals and Antimicrobial Activities of *Rumex* nervosus Natural Populations Grown in Sarawat Mountains, Kingdom of Saudi Arabia, *Arabian J. Sci. Eng*., 2018, **43**, 3465–3476. doi: 10.1007/s13369-018-3136-z
18. M. Al-Nowihi, A. Faisal and G. Al-Asbahi, Antimicrobial activity of *Rumex* nrvosus extract collected from Yemen against local selected isolates pathogens, *J. Microbiol. Exp*., 2020, **8**, 93–96. doi: 10.15406/jmen.2020.08.00291
19. K. Hossam, F. Bouhlal, L. Hermouche, I. Merimi, N. Labjar, A. Chaouiki and S. El Hajjaji, Understanding Corrosion Inhibition of C38 Steel in HCl Media by Omeprazole: Insights for Experimental and Computational Studies, *J. Fail. Anal. Prev*., 2020, **21**, 213–227. doi: 10.1007/s11668-020-01042-1
20. N.A.A. Ali, W.-D. Jülich, C. Kusnick and U. Lindequist, Screening of Yemeni medicinal plants for antibacterial and cytotoxic activities, *J. Ethnopharmacol*., 2001, **74**, 173–179. doi: 10.1016/S0378-8741(00)00364-0
21. C. Wang, J. Chen, J. Han, C. Wang and B. Hu, Enhanced corrosion inhibition performance of novel modified polyaspartic acid on carbon steel in HCl solution, *J. Alloys Compd*., 2019, **771**, 736–746. doi: 10.1016/j.jallcom.2018.08.031
22. A. Molhi, R. Hsissou, M. Damej, A. Berisha, V. Thaçi, A. Belafhaili and S. El Hajjaji, Contribution to the corrosion inhibition of C38 steel in 1 M hydrochloric acid medium by a new epoxy resin PGEPPP, *Int. J. Corros. Scale Inhib*., 2021, **10**, 399–418. doi: 10.17675/2305-6894-2021-10-1-15
23. X. Zheng, S. Zhang, M. Gong and W. Li, Experimental and Theoretical Study on the Corrosion Inhibition of Mild Steel by 1-Octyl-3-methylimidazolium l-Prolinate in Sulfuric Acid Solution, *Ind. Eng. Chem. Res*., 2014, **53** 16349–16358. doi: 10.1021/ie50257\8q
24. B. Gómez, N.V. Likhanova, M.A. Domínguez-Aguilar, R. Martínez-Palou, A. Vela and J.L. Gázquez, Quantum Chemical Study of the Inhibitive Properties of 2-Pyridyl-Azoles, *J. Phys. Chem. B*, 2006, **110**, 8928–8934. doi: 10.1021/jp057143y
25. A. Popova, Temperature effect on mild steel corrosion in acid media in presence of azoles, *Corros. Sci*., 2007, **49**, 2144–2158. doi: 10.1016/j.corsci.2006.10.020

26. M. Pauli, A.M.C. Gomes, R.L. Cavalcante, R.B. Serpa, C.P.S. Reis, F.T. Reis and M. Sartorelli, Capacitance spectra extracted from EIS by a model-free generalized phase element analysis, *Electrochim. Acta*, 2019, **320**, 134366. doi: 10.1016/j.electacta.2019.06.059
27. H.H. Hernández, A.M.R. Reynoso, J.C.T. González, C.O.G. Morán, J.G.M. Hernández A.M. Ruiz and R.O. Cruz, *Electrochemical Impedance Spectroscopy (EIS): A Review Study of Basic Aspects of the Corrosion Mechanism Applied to Steels*, IntechOpen, 2020. doi: 10.5772/intechopen.94470
28. F. Bouhlal, N. Labjar, F. Abdoun, A. Mazkour, M. Serghini-Idrissi, M. El Mahi, and S. El Hajjaji, Electrochemical and Thermodynamic Investigation on Corrosion Inhibition of C38 Steel in 1M Hydrochloric Acid Using the Hydro-Alcoholic Extract of Used Coffee Grounds, *Int. J. Corros*., 2020, **2020**, 4045802. doi: 10.1155/2020/4045802
29. R. Cabrera-Sierra, I. García, E. Sosa, T. Oropeza and I. González, Electrochemical behavior of carbon steel in alkaline sour environments measured by electrochemical impedance spectroscopy, *Electrochim. Acta*, 2000, **46**, 487–497. doi: 10.1016/S0013-4686(00)00567-3
30. M.T. Majd, M. Ramezanzadeh, B. Ramezanzadeh and G. Bahlakeh, Production of an environmentally stable anti-corrosion film based on Esfand seed extract molecules-metal cations: integrated experimental and computer modeling approaches, *J. Hazard. Mater*., 2020, **382**, 121029. doi: 10.1016/j.jhazmat.2019.121029
31. D.A. Lopez, S.N. Simison and S.R. De Sanchez, The influence of steel microstructure on CO_2 corrosion. EIS studies on the inhibition efficiency of benzimidazole, *Electrochim. Acta*, 2003, **48**, 845–854. doi: 10.1016/S0013-4686(02)00776-4
32. L.O. Olasunkanmi, M.M. Kabanda and E.E. Ebenso, Quinoxaline derivatives as corrosion inhibitors for mild steel in hydrochloric acid medium: Electrochemical and quantum chemical studies, *Phys. E (Amsterdam, Neth.)*, 2016, **76**, 109–126. doi: 10.1016/j.physe.2015.10.005
33. Y. Qiang, S. Zhang, B. Tan and S. Chen, Evaluation of Ginkgo leaf extract as an eco-friendly corrosion inhibitor of X70 steel in HCl solution, *Corros. Sci*., 2018, **133**, 6–16. doi: 10.1016/j.corsci.2018.01.008
34. R. Karthikaiselvi and S. Subhashini, Study of adsorption properties and inhibition of mild steel corrosion in hydrochloric acid media by water soluble composite poly (vinyl alcohol-omethoxy aniline), *J. Assoc. Arab Univ. Basic Appl. Sci*, 2018, **16**, 74–82. doi: 10.1016/j.jaubas.2013.06.002
35. D.B. Hmamou, R. Salghi, A. Zarrouk, H. Zarrouk, M. Errami, B. Hammouti, L. Bazzi and L. Bazzi, Adsorption and corrosion inhibition of mild steel in hydrochloric acid solution by verbena essential oil, *Res. Chem. Intermed*., 2013, **39,** 973–989. doi: 10.1007/s11164-012-0609-7

36. O. Sanni, A.P.I. Popoola and O.S.I. Fayomi, Temperature Effect, Activation Energies and Adsorption Studies of Waste Material as Stainless Steel Corrosion Inhibitor in Sulphuric Acid 0.5 M, *J. Bio Tribo Corros*., 2019, **5**, 88. doi: 10.1007/s40735-019-0280-2
37. S. Martinez and I. Stern, Thermodynamic characterization of metal dissolution and inhibitor adsorption processes in the low carbon steel/mimosa tannin/sulfuric acid system, *Appl. Surf. Sci*., 2002, **199**, 83–89. doi: 10.1016/S0169-4332(02)00546-9
38. E.A. Noor and A.H. Al-Moubaraki, Thermodynamic study of metal corrosion and inhibitor adsorption processes in mild steel/1-methyl-4[4′(-X)-styryl pyridinium iodides/hydrochloric acid systems, *Mater. Chem. Phys*., 2008, **110**, 145–154. doi: 10.1016/j.matchemphys.2008.01.028
39. A. Bousskri, A. Anejjar, M. Messali, R. Salghi, O. Benali, Y. Karzazi and B. Hammouti, Corrosion inhibition of carbon steel in aggressive acidic media with 1-(2-(4-chlorophenyl)-2-oxoethyl)pyridazinium bromide, *J. Mol. Liq*., 2015, **211**, 1000–1008. doi: 10.1016/j.molliq.2015.08.038

♦ ♦ ♦